JOURNAL OF GEOPHYSICAL RESEARCH, VOL. 90, NO. B7, PAGES 5479–5495, JUNE 10, 1985

Second-Order Moment of Central California Seismicity, 1969–1982

PAUL REASENBERG

U.S. Geological Survey, Menlo Park, California

The second-order moment (cross-correlation function) of earthquakes in the U.S. Geological Survey central California catalog between 1969 and 1982 was calculated with respect to a magnitude threshold $M \geq 4.0$ over interevent distances up to 80 km and interevent times up to 320 days. The statistical procedure results in a representation of the spatial-temporal structure of the catalog associated with $M \geq 4.0$ earthquakes and is capable of revealing patterns too weak to be detected in the space-time distribution of seismicity for individual earthquake sequences. A method is introduced for identifying aftershocks based on a physical two-parameter model of the earthquake interaction process. The results show that the aftershock process dominates the second-order moment and may even obscure the statistical expression of a precursory process. A concentration of foreshocks within 15 km and 3 days of $M \geq 4.0$ main shocks exhibits an apparent migration toward the main shock loci with velocity 2.6–5.3 km/d. This concentration may be related to an observed tendency for $M \geq 4.0$ events to cluster (autocorrelate) over this interevent range. With the identified aftershocks removed, the residual catalog is Poissonion in space and time. When two $M \geq 4.0$ earthquakes occur within 80 km and 40 days of each other, aftershock productivity appears to be relatively enhanced in the earlier sequence. This suggests that aftershock populations are not solely dependent on their main shocks and that unusually productive aftershock sequences may be predictors of future moderate earthquakes.

INTRODUCTION

The nature of seismicity patterns prior to moderate and large earthquakes has been a subject of continuing and widespread investigation. With the emergence during the past few decades of instrumental earthquake catalogs including small-magnitude events, studies of the distribution of earthquakes in space, time, and size, employing statistical or pattern analysis methods, have dominated this field of investigation. By far the most commonly investigated seismicity patterns are those in space and time before moderate and large earthquakes. Research in this area was recently summarized by *Kanamori* [1981], who concluded that, in general, seismicity patterns vary substantially from event to event, even though some of the fundamental physical processes leading to an earthquake may be common to all events. He postulated that fault zone heterogeneity and complexity are responsible for the observed variations.

Two distinct meanings of the term "pattern" are currently in use in earthquake prediction literature. Usually the term means "a particular design composed of a number of elements in a regular or formal manner." Accordingly, most seismicity pattern studies gather data on the distribution of earthquakes in space, time, and size (hereafter referred to as the first-order moment), examining seismicity rate, location, and migration of foreshocks and aftershocks, gaps, donuts, and variations in b value [*Kanamori*, 1981, and references therein]. In some cases, subjectively recognizable patterns (e.g., foreshock cluster, gap, b value anomaly) are observed that closely resemble those predicted for various theories of seismogenesis; in other cases none are observed. Such variation seems to be the rule rather than the exception and limits the usefulness of these patterns for both prediction of earthquakes and testing of seismogenic theory. Another meaning of the term is "a mode of behavior, arrangement, or design characteristic of things." Such patterns are by definition common or coherent among many individual cases (earthquake sequences). Coherent precursory patterns in seismicity, if they are present at all, are certainly weak, and their detection is difficult. The problem of detecting a weak coherent pattern among many earthquake sequences, in the presence of great variation among the individual sequences, is analogous to the one-dimensional problem of time-sequence signal detection in the presence of random noise. Just as stacking in the one-dimensional case enhances the signal-to-noise ratio, analysis of the higher-order statistical moments of an earthquake catalog may enhance coherent patterns that are too weak to be detected in the first-order moment. Analysis of the second-order moment (formally defined in the following section) is a relatively new and powerful statistical method for identifying coherent seismicity patterns [*Kagan and Knopoff*, 1976]. As we will see below, there is a close correspondence between the time-sequence stack and certain projections of the second-order moment.

The second-order moment (also called the two-point correlation function) is used to describe the pairwise statistical interdependence of earthquakes. Because the elemental unit of earthquake interaction is an earthquake pair, the second-order moment is well suited to detect coherent precursory pairwise patterns in foreshock-main shock pairs of events. Statistical relationships involving three or more earthquakes, which may be represented by higher-order statistical moments [*Kagan*, 1981*a*, *b*], are not considered in this study. *Kagan and Knopoff* [1976] examined second-order autocorrelation and cross-correlation functions for a 60-year worldwide catalog of 1339 large ($M \geq 7$) earthquakes, for various depth ranges and over interevent distances up to 2500 km and times up to 10 years. They found the distribution of epicenters to be significantly nonrandom on this scale and consistent with models of epicenter migration and rarefaction in activity (gaps) preceding and following large earthquakes. *Vere-Jones* [1978] identified features in the second-order moment of 10,000 microearthquakes recorded over a 15-year period in Japan that he tentatively associated with precursory swarms, "hot spots," and migration.

In this study, selected projections of the second-order moment of earthquakes in the U.S. Geological Survey central California catalog are examined for patterns indicating a coherent departure from random occurrence. The detailed structure of the second-order moment for central California seismicity is analyzed in terms of two-event interaction processes.

Paper number 4B5271.

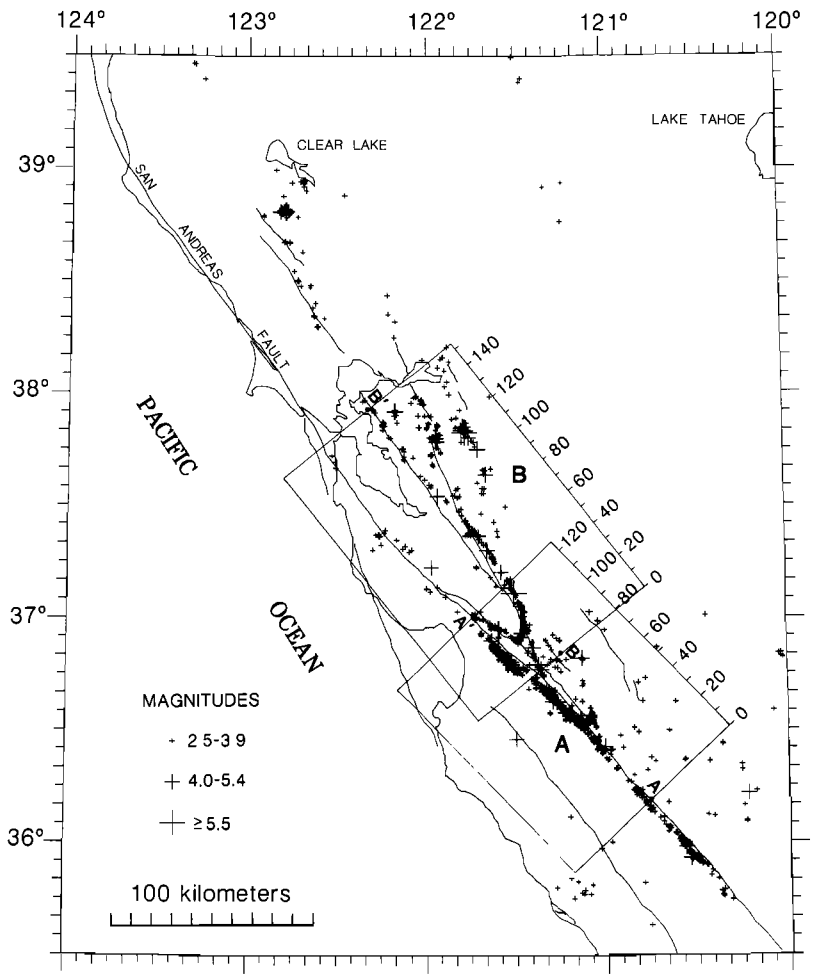

Fig. 1. Earthquakes with $M \geq 2.5$ between 1969 and 1982 within the study area. The coastline of California and major faults are indictated by solid lines. Boxes A and B indicate the epicentral areas represented in Figures 8 and 10 and Figures 9 and 11, respectively. Scales on boxes are in kilometers and coincide with distance scales in Figures 8–11. Data used in study include these events and events with $M < 2.5$ not shown.

In order to isolate the strong statistical expression of aftershocks from the second-order moment, thereby allowing weaker seismogenic processes to be revealed, a new method for identifying dependent earthquakes (clusters) based on a physical model of earthquake interaction is introduced and applied to the catalog, and the resulting catalog is then reanalyzed.

Data

The set of earthquakes used in this study was selected from the U.S. Geological Survey (USGS) central California catalog within the area shown in Figure 1 for the period January 1, 1969, to December 31, 1982. The locations for 1978 and later in the raw catalog are considered preliminary (hypocenters may be revised). Thus it is likely that some large errors in location may be included in this period. The influence of location errors in the catalog upon the second-order moment was shown by *Kagan and Knopoff* [1980] to be significant for interevent distances comparable to the location errors. Therefore, in order to use both final and preliminary locations in the catalog only HYPO71 quality A and B solutions were selected. The selected set is essentially homogeneous in location error. Ninety five percent of the included events for the entire period have estimated epicentral uncertainty ERH $\leq$ 1.0 km. For the periods 1969–1977 and 1978–1982 the corresponding percentages are 96 and 95, respectively. It is possible that the preliminary nature of the catalog for 1978–1982 might result in a reduction in the magnitude level of completeness for that period. This could occur if a significant number of preliminary C or D quality solutions are to be later revised to A or B quality. The minimum magnitude of completeness was estimated for consecutive 1-year intervals as the magnitude at which the log cumulative number of events departs from a linear magnitude dependence. Least squares linear regression of the results reveals a decrease is the completeness level from 1.75 in 1969 to 1.25 in 1982. The decrease is presumably a consequence of the increase in network station density over that period. However, no abrupt change in completeness level occurs at the 1977–1978 seam, suggesting that the detection ability of the network for well-located (quality A and B) solutions is unchanged across this seam.

I depart from the usual procedure [*Kagan and Knopoff*, 1978, 1980; *Vere-Jones*, 1978] by not discarding events with magnitudes below the estimated completeness level. As a consequence of including events in magnitude ranges thought to be incomplete in the catalog, it will be necessary to refrain from later making inferences that assume completeness.

Method of Second-Order Moments

I model seismogenesis as a point process in five-dimensional position-magnitude-time space S. The application to seismology of point processes and the second-order moment is intro-

duced and investigated with regional and worldwide catalogs by *Kagan and Knopoff* [1976, 1980], *Vere-Jones* [1970, 1978], and *Daley and Vere-Jones* [1972]. The jth earthquake e_j in the catalog is represented by a five-element vector

$$\mathbf{x}_j = x_j^k \qquad k = 1, 5$$

where (x_j^1, x_j^2) specifies the epicenter, x_j^3 the depth, x_j^4 the magnitude, and x_j^5 the origin time. The first-order moment $m_1(\mathbf{x})$ of the process is simply the expectation value of the number of events with parameters $\mathbf{x}$. For a point process the moment is discrete and is calculated by summation [*Kagan and Knopoff*, 1976; *Cox and Lewis*, 1966]. The first-order moment is a complete description of the distribution of the individual events in the catalog.

The second-order moment $m_2(\mathbf{x}_1, \mathbf{x}_2)$ is expressed as [*Kagan and Knopoff*, 1976; *Cox and Lewis*, 1966]

$$m_2(\mathbf{x}_1, \mathbf{x}_2) = m_1(\mathbf{x}_1) \cdot m(\mathbf{x}_2|\mathbf{x}_1) \tag{1}$$

where $m(\mathbf{x}_2|\mathbf{x}_1)$ is the conditional moment of the process, i.e., the expectation value of the number of events with parameter $\mathbf{x}_2$ given that another event at $\mathbf{x}_1$ has occurred. The second-order moment is the two-point correlation function and describes the distribution of pairs of events in the catalog. That is, $m_2(\mathbf{x}_i, \mathbf{x}_j)$ is equal to the expectation value of the number of earthquake pairs (e_i, e_j). In practice, $m_2(\mathbf{x}_i, \mathbf{x}_j)$ is calculated by summation over the catalog. When e_i and e_j are drawn from the same population, m_2 is the autocorrelation matrix and is symmetric with respect to i and j. When e_i and e_j are drawn from nonintersecting subsets of the catalog, m_2 is a (nonsymmetric) cross-correlation matrix.

I now introduce several simplifications to m_2. Some result directly from assumptions about the physics of the seismogenic process; others are arbitrary and for convenience. First, because the estimated errors in hypocentral depth are appreciable relative to the range of depths in the catalog, depth is not used in the analysis; interevent distances are calculated between epicenters.

Second, to simplify the magnitude relation of pairs, m_2 is formed from complementary subsets $[e_i]$ and $[e_j]$ defined with respect to a fixed magnitude threshold M_c. That is, for e_i, $M \geq M_c$, while for e_j, $M < M_c$; all such pairs are counted. M_c is chosen sufficiently high that the primary events are interesting but not so high that their number is too small to draw statistically significant inferences. In the present study, $M_c = 4.0$, resulting in 46 primary events, 40,370 secondary events, and 1,857,020 potential pairs.

Next, I assume that the physical process underlying the catalog is stationary over the duration of the catalog so that the absolute origin times x_i^5 and x_j^5 may be replaced without loss of information by the time difference Δt_{ij} between events.

Finally, two assumptions simplify the spatial relationship of pairs. Each results in the substitution for the absolute epicentral coordinates with a measure of relative position between events in the pair. First, I assume spatial homogeneity of the seismogenic process. The position of the events in each pair is then replaced by the distance between them. That is, $\Delta r_{ij} = [(x_i^1 - x_j^1)^2 + (x_i^2 - x_j^2)^2]^{1/2}$. However, even to first order this assumption is obviously incorrect. Earthquakes within the study area align in narrow zones subparallel to the northwest-southeast trending San Andreas fault system. Because the distribution likely results from the dynamics of seismogenesis (i.e., strike-slip movement in the fault system), it is reasonable to assume that this direction may also be preferred for earthquake interaction. One can take advantage of this relationship by projecting each epicenter onto a straight line approximately parallel to the San Andreas fault system in central California and define Δl_{ij} as the scalar position on the line of one event in the pair relative to the other. That is,

$$\Delta l_{ij} = [(x_i^1 - x_j^1)^2 + (x_i^2 - x_j^2)^2]^{1/2} \cos(\alpha_{ij} - \alpha_0) \tag{2}$$

where

$$\alpha_{ij} = \tan^{-1}[(x_i^2 - x_j^2)/(x_i^1 - x_j^1)] \tag{3}$$

and α_0 is the average strike (N36°W) of the San Andreas fault in central California. The first simplification assumes complete isotropy ($\Delta r_{ij} = \Delta r_{ji}$), while in the second, one-dimensional anisotropy (along the fault) is imposed ($\Delta l_{ij} = -\Delta l_{ji}$). The second-order moments thus formed are referred to as $m_{2r}(\Delta r, \Delta t;\ M_c = 4.0)$ and $m_{2l}(\Delta l, \Delta t;\ M_c = 4.0)$, respectively. In the following section m_{2r} and m_{2l} are calculated for the central California catalog, and their structure is examined for evidence of earthquake interaction processes.

Results for the Central California Catalog

In this study I examine m_{2r} and m_{2l} for central California seismicity (1969–1982) over interevent times of 1/4 day to 320 days and for interevent distances of 0.5 km to 80 km. These ranges are most likely to contain structure indicative of a physical precursory process for $M \geq 4.0$ events. Figure 2 shows a portion of the cross-correlation matrix m_{2l}. Elements in the upper (lower) half of Figure 2 represent pairs in which the smaller event is southeast (northwest) of the larger event. Elements on the left (right) represent foreshock-main shock (main shock-aftershock) pairs. Thus the value 4 of the encircled element in Figure 2 means that four earthquake pairs exist in the catalog for which one earthquake ($M < 4.0$) precedes another ($M \geq 4.0$) by between 6 and 7 days and is located 8–10 km southeast of it (measured along the fault strike). Figure 2 is equivalent to a two-dimensional stack of separate space-time plots in the vicinity of each ($M \geq 4.0$) main shock, with the main shocks aligned at the axis origin and with cumulative counts of foreshocks and aftershocks in each relative time and space interval replacing the epicenter symbols. An advantage of studying this form of the second-order moment is that coherent patterns in the seismicity not strong enough to be recognized in space-time plots of individual events constructively add and may become apparent in the stack. Use of the terms "foreshock" and "aftershock" in this context refers only to the magnitude and time relationships of two events and does not necessarily imply a causal or physical relationship.

The quantities m_{2r} and m_{2l} were calculated for the central California catalog over several interevent distance and time windows and are shown in Figures 3–7, with the counts of each bivariate interval represented by contours. The windows are overlapping, and selected overlap areas are indicated for orientation. Figures 3–5 progressively focus in on the main-shock region, while Figures 5–7 examine the smallest spatial window over increasing interevent times. The central portion of Figure 3*b* corresponds to the result shown in Figure 2. The temporal and spatial correlation of earthquakes shown in Figures 3–7 are obtained from the observed rates

$$n(\Delta t) = \sum_{\Delta l} m_{2l}(\Delta l, \Delta t) \tag{4}$$

$$n(\Delta l) = \sum_{\Delta t} m_{2l}(\Delta l, \Delta t) \tag{5}$$

respectively, and are shown projected along the appropriate axes in each figure. The spatial density is shown separately for

Interevent Time Δt (days)

Interevent Position Δl(km)

Δl (km)	-10	-9	-8	-7	-6	-5	-4	-3	-2	-1	1	2	3	4	5	6	7	8	9	10	Poisson Rate
24	1	1	2	1	2	4	8+	3	3	3	1	9+	3	3	4	3	2	3	3	1	2.64
22	5	1	1	1	1	0	0	1	2	1	2	5	0	0	0	0	2	1	3	3	2.11
20	0	6	1	5	1	9+	1	2	0	5	0	2	3	2	4	1	2	2	1	3	3.16
18	1	2	8*	1	2	5	2	2	1	1	2	4	2	3	4	3	6	2	0	5	2.99
16	1	1	0	0	6	0	1	0	5	6	6	11+	6	14+	5	3	1	7+	3	4	2.91
14	2	2	1	0	1	2	2	6	2	3	10+	17+	18+	2	4	0	3	9+	2	10+	2.63
12	5	2	0	2	2	0	2	4	2	3	16+	25+	23+	122	39+	48+	24+	13*	8	14*	7.13
10	5	6	4	(4)	0	3	4	77+	46+	30+	28+	19+	25+	35+	12	26+	30+	11	5	9	7.99
8	2	4	2	3	4	1	1	11*	27+	17+	36+	25+	21+	9	7	1	5	7	4	1	4.88
6	5	5	0	2	3	5	1	1	14+	7	44+	23+	26+	15+	9	10*	11*	11*	7	3	4.88
4	12*	6	3	1	8	3	1	2	1	13*	86+	66+	51+	19+	13*	11	15+	8	3	1	6.61
2	16	17	14	11	13	8	4	10	15	169+	615+	142+	104+	62+	53+	42+	38	37	37	26	28.73
-2	15	11	13	11	93+	28	17	7	21	179+	665+	158+	170+	87+	58+	46+	42	32	29	32	34.81
-4	7	3	4	2	18*	17*	10	7	15	36+	177+	46+	37+	36+	16*	20+	9	6	19+	17*	9.98
-6	0	5	1	1	2	6	2	3	3	4	126+	14+	27+	25+	14+	7	6	12*	9	11*	5.45
-8	1	1	3	0	0	3	5	5	8*	8*	34+	3	6	14+	7	5	2	5	5	3	3.31
-10	0	7	3	1	0	3	10+	9+	12+	14+	12+	4	1	5	11+	8*	8*	15+	5	1	3.42
-12	0	2	3	1	3	2	33+	32+	27+	18+	19+	7	14+	5	17+	10*	6	3	6	1	4.61
-14	0	2	0	0	0	4	38+	90+	45+	19+	17+	9	17+	7	11*	7	14+	12*	4	1	5.56
-16	0	0	1	1	1	0	31+	26+	10+	13+	9+	7	1	4	12+	7	14+	10+	4	4	3.44
-18	0	0	2	0	0	2	4	2	6*	9+	10+	2	1	10+	9+	3	3	0	3	4	2.42
-20	1	0	1	0	3	2	4	1	2	3	0	1	1	5	6*	3	6	4	2	1	2.47
-22	3	0	1	1	8+	1	3	0	0	5	2	4	3	2	5	0	1	2	2	2	2.26
-24	2	2	2	0	4+	6+	1	1	2	3	3	7+	0	2	1	1	2	4	3	0	1.64

Fig. 2. Portion of the second-order moment m_{2l} calculated over incremental steps in Δl of 2 km and in Δt of 1 day. Vertical and horizontal lines indicate position of $\Delta t = 0$ and $\Delta l = 0$, respectively. Entry in each (Δl, Δt) cell is the number of pairs of earthquakes in the catalog with interevent separation Δl and time difference Δt. For each row, entry in column on right is the mean occurrence rate of pairs with corresponding interevent separation Δl (i.e., entry is mean of entire row). Asterisk indicates entry whose probability of occurrence in a Poisson process with rate equal to mean observed rate is less than 0.05; plus sign indicates entry with Poisson probability less than 0.01. Results in this figure are also represented in center portion of Figure 3*b*.

all Δt, for $\Delta t < 0$ (foreshock-main shock pairs) and for $\Delta t > 0$ (main shock-aftershock pairs).

Each time series $n_{\Delta l}(\Delta t)$, represented by a single row in Figure 2 (Δl = constant), is tested against the null hypothesis of a Poissonian distribution with parameter derived from the observations using the chi-square test. For all values of $\Delta l < 20$ km, the null hypothesis is rejected at the 99.9% confidence level, in agreement with previous results showing the non-Poissonian nature of seismicity [*Schlien and Toksoz*, 1970; *Gardner and Knopoff*, 1974].

Visual inspection of m_{2l} and m_{2r} reveals four dominant features in central California seismicity (Figures 3–7). First, the main shock-aftershock pair population is concentrated in the region $\Delta r < 20$ km, reflecting the spatial extent of the larger earthquake sequences in the catalog (six of the 46 primary events have magnitude $5.0 \leq M \leq 5.9$). The overall apparent diminution with time of the spatial extent of the aftershock zone contrast with previous observations of aftershock zone growth [*Ellsworth*, 1975; *Wesson*, 1983] and shows that if spatial expansion of aftershock zones is a common pattern, it is a weak one obscured in the second-order moment by variations in the individual sequences. On the basis of a related approach and using a worldwide catalog, *Prozorov and Dziewonski* [1982] constructed a filter designed to isolate aftershock clusters by using a window that closely resembles this form.

A second apparent feature of m_{2l} and m_{2r} is an exponentiallike increase in the foreshock rate within approximately 4 km and 1 day of main shocks (Figure 5). The size and duration of this feature appears artificially enlarged in Figures 3, 4, 6, and 7 due to the fact that cell sizes used in these larger-scale calculations of m_2 equal or exceed the size of the feature.

Also within this distance (4 km) of main shocks appears a prominent and continuing concentration of foreshocks over at least 10 months (Figure 7*b*). There is no apparent character-

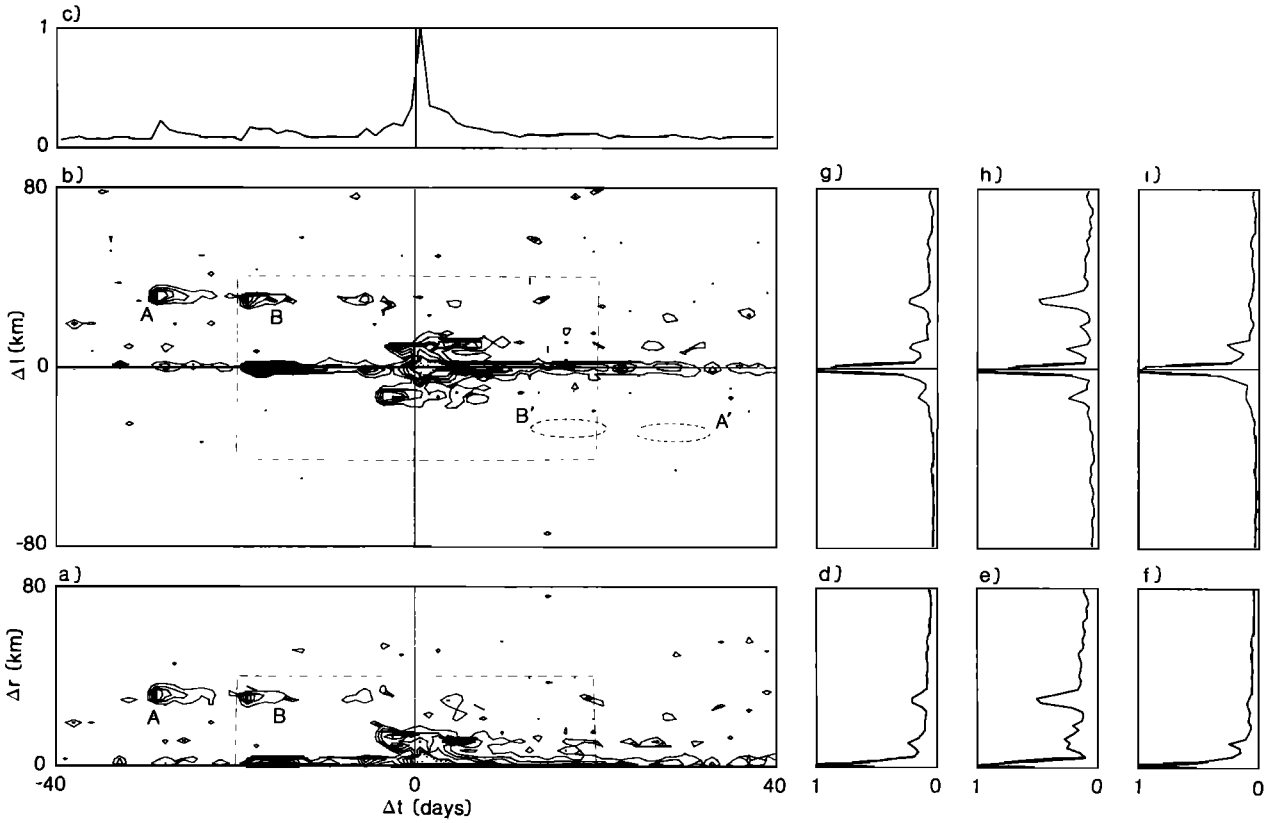

Fig. 3. (*a*) Second-order moment m_{2r} calculated for the window $0 \leq \Delta r \leq 80$ km, $-40 \leq \Delta t \leq 40$ days, on a 40 (Δr) by 80 (Δt) grid, shown as contours of number of pairs in the catalog with interevent distance Δr and interevent time Δt. Each grid point corresponds to a cell 2 km by 1 day. Contour interval is 10. Shading indicates areas with values greater than five contours. Dashed box indicates ranges of moment shown in Figure 4*a*. Features labeled with a capital letter in Figures 3–5 are discussed in the text. (*b*) Second-order moment m_{2l} calculated for the window $-80 \leq \Delta l \leq 80$ km, $-40 \leq \Delta t \leq 40$ days, on an 80 by 80 grid, shown as contours of number of pairs in the catalog with relative position on the fault Δl and interevent time Δt (see text). Each grid point corresponds to a cell 2 km by 1 day. Contour interval is 8. Shading indicates areas with values greater than five contours. Δl positive (negative) corresponds to pairs in which the smaller event is southeast (northwest) of the main shock. Δt positive (negative) corresponds to main shock-aftershock (foreshock-main shock) pairs. Dashed box indicates ranges of moment shown in Figure 4*b*. (*c*) Temporal correlation of earthquakes as a function of interevent time Δt, obtained by summation of columns in Figure 3*b*. Time axis corresponds with Figures 3*a* and 3*b*. (*d*) Spatial correlation of earthquakes as a function of interevent distance Δr, obtained by summation of rows in Figure 3*a*. Relative distance axis corresponds with Figure 3*a*. (*e*) Same as Figure 3*d*, but calculated only for foreshock-main shock pairs. (*f*) Same as Figure 3*d*, but calculated only for main shock-aftershock pairs. (*g*) Spatial correlation of earthquakes as a function of relative position along fault Δl (see text), obtained by summation of rows in Figure 3*b*. Relative distance axis corresponds with Figure 3*b*. (*h*) Same as Figure 3*g*, but calculated only for foreshock-main shock pairs. (*i*) Same as Figure 3*g*, but calculated only for main shock-aftershock pairs.

istic time constant associated with this spatial concentration. This observation is consistent with the interpretation that $M \geq 4.0$ main shocks preferentially occur in areas of perennially high seismicity ("hot spots") on the fault [*Wesson and Ellsworth*, 1973].

Finally, note the prominence of several isolated clusters of pairs in m_{2l} labeled A–F in Figures 3–5. Owing to their temporal and spatial proximity to main shocks, clusters C and D at -5 days $< \Delta t < 0$ and $\Delta l < 15$ km appear to be microseismic precursors to the main shock. In m_{2r} these features combine (Figure 5*a*) to form an apparent migration toward the main shock with velocity between 2.6 and 5.3 km/d. If a coherent enhancement of microseismicity occurred with such a relationship to all $M \geq 4$ main shocks, the resulting patterns in m_{2l} and m_{2r} would be similar indeed to these observed features. However, detailed examination of the catalog reveals that many of these pair clusters consist of only one or a few main shocks paired with aftershocks of another main shock located nearby in space and time. Of the 209 pairs in cluster B (Figure 3*b*), 88% consist of a San Juan Bautista event (720923 1507, M 4.1) paired with an aftershock of the Stone Canyon sequence (720904-05, M 4.6) 30 km to the southeast. Similarly, of the 480 pairs in cluster A (Figure 3*b*), over 95% consist of the main shock (721003), M 4.8) at San Juan Bautista paired with an aftershock of the Stone Canyon event. Thus A and B are "images" of particular aftershock sequences and probably do not represent a general pattern of foreshocks. A similar result was found for all the clusters labeled in Figures 3–5. These examples serve to illustrate that aftershocks strongly affect the structure of the second-order moment and dictate the need for caution in ascribing significance to "foreshocklike" patterns.

In the case of clusters involving an $M \geq 4.0$ event paired with aftershocks of another $M \geq 4.0$ event, a symmetrically located cluster at ($\Delta l' = -\Delta l$, $\Delta t' = -\Delta t$) corresponds to pairs formed with the main shock roles reversed. In the case of clusters A and B the corresponding images at $\Delta t > 0$ (A′ and B′ in Figure 3*b*) contain fewer than 25 and 28 pairs, respec-

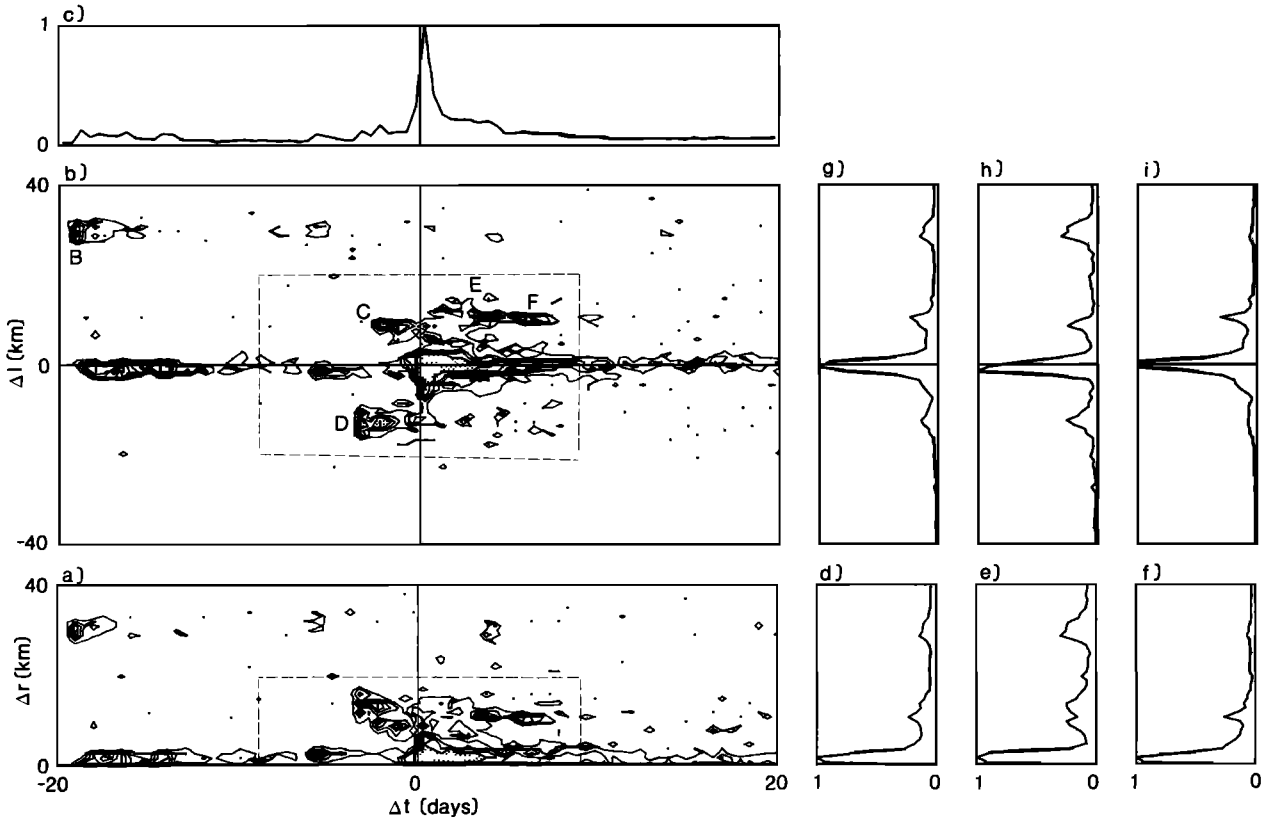

Fig. 4. Second-order moments and correlation functions for the ranges indicated by dashed boxes in Figure 3. Dashed boxes indicate ranges shown in Figure 5. Cell size 1 km by 0.5 day in Figures 4*a* and 4*b*. Contour interval is 5 in Figure 4*a* and 4 in Figure 4*b*. See Figure 3 for further explanation.

tively. Inspection of Figures 3–7 suggests that, in general, the earlier of clustered clusters may have a larger aftershock population than the later one. *Keilis-Borok et al.* [1980] observed a similar pattern over larger distances and time differences between intensely populous aftershock sequences ("bursts of aftershocks") and subsequent larger ($M > 6.5$) main shocks in southern California.

The prevalence of cluster features in the second-order moment related to aftershock sequences suggests that the aftershock process effectively dominates the second-order moment of the catalog and may obscure other, if any, statistical patterns present in the seismicity. While we have identified the most obvious aftershock-related pair clusters, numerous smaller ones exist throughout the second-order moment. Therefore, before further analyzing the pair statistics of the catalog, it is desirable to identify independently the aftershocks to that they may be statistically treated as nonindependent events.

Identification of Aftershocks

Some previous methods for identifying and removing aftershocks have modeled the total extent of aftershock zones with a rectangular window ($0 < \Delta t < T$, $0 < \Delta r < R$), where T and R are functions of the main shock magnitude [*Gardner and Knopoff*, 1974; *Knopoff and Gardner*, 1972; *Keilis-Borok et al.*, 1980]. T and R are defined sufficiently large as to include most of the aftershocks for any sequence of a given magnitude. However, because the spatial and temporal extents of aftershock sequences vary widely from event to event, these methods necessarily overestimate the aftershock population in nearly all cases. This shortcoming makes these methods generally inadequate for accurate identification of aftershocks. *Savage* [1972] identified clusters of earthquakes in Nevada by associating events separated in space and time by less than arbitrarily selected limits of 10 min and a few hundred meters. His method had the advantage of not imposing a window for the final size or shape of the cluster, thereby allowing the distribution of seismicity to define them. *McNally* [1976] applied a cluster criterion based only on interevent time that varied according to changes in the long-term rate of seismicity. This method ignored the spatial distribution of earthquakes.

In this study I identify aftershock populations by modeling an interaction zone about each earthquake in the catalog with a method similar to the one developed by *Savage* [1972]. I assume that any earthquake that occurs within the interaction zone of a prior earthquake is an aftershock and should therefore be considered statistically dependent on it. Events thus associated are referred to as belonging to a cluster. The clusters grow by simple rules of association. When an independent event (one not yet associated with a cluster) is associated with a previously clustered event, it becomes a member of the existing cluster. When two events belonging to different clusters are associated, the respective clusters are redefined as one cluster. When two independent events are associated, they form a new cluster.

The interaction zones are dynamically modeled with one spatial and one temporal parameter. The cluster algorithm associates two earthquakes if their hypocentral and origin time difference are respectively less than the spatial and temporal extent of the interaction zone modeled for the first-occurring event. The spatial extent of the interaction zone is

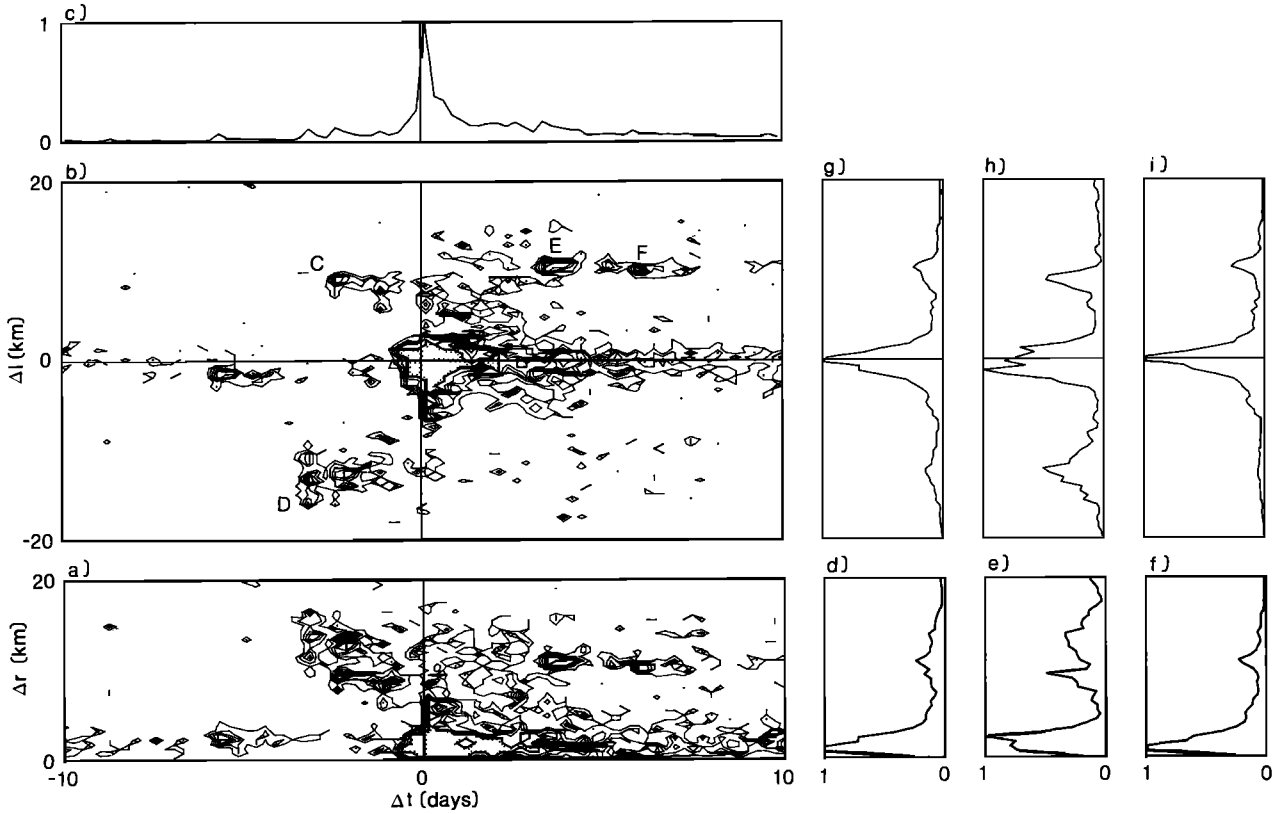

Fig. 5. Second-order moments and correlation functions for the ranges indicated by dashed boxes in Figure 4. Cell size 0.5 km by 0.25 day in Figures 5*a* and 5*b*. Contour interval is 2 in Figures 5*a* and 5*b*. See Figure 3 for further explanation.

based on an estimate of stress redistribution in the vicinity of each earthquake. While the stress state has contributions from the stress perturbations from all previous earthquakes as well as the "preexisting" stress, I assume that the two strongest contributors are the stress redistributions from the most recent (current) event and from the largest previous event in the current sequence and ignore other contributions to the stress state. The length scale for modeling the interaction zones is based on source dimensions. To model the effect of stress-relieving processes such as afterslip, the contribution from the most recent event is scaled by its source dimension times a parameter Q and that of its largest ancestor simply by its source dimension. The source dimension for each event is estimated by the radius of a circular crack [*Kanamori and Anderson*, 1975] corresponding to the event's moment M_0, assuming a stress drop of 30 bars. The moment is obtained from the USGS Coda magnitude M using the relation

$$\log M_0 = 17 + 1.2M \tag{6}$$

[*Bakun*, 1984]. For example, for $Q = 10$, resulting interaction zone sizes are 0.7 and 4.6 km for M 2.0 and M 4.0 events, respectively.

The assumptions made in formulating the spatial extent of the interaction zone are certainly oversimplified. However, experimentation with varying these parameters shows that both the number of clusters identified and the total number of earthquakes associated with a cluster are remarkably insensitive to variations in the parameters defining the interaction zones. Other factors believed to influence the occurrence of earthquakes, including the state of stress prior to 1969, geometric barriers, and rock strength heterogeneity have been ignored in the model. While these factors undoubtedly play an important role in the seismogenic process, their detailed effects are largely unknown. Not including them in the model allows the possibility of later inferring some of them from the particular pattern of clusters formed with this simple model.

The temporal extent of the interaction zone is determined with a probabilistic model. For an earthquake previously associated with an aftershock sequence, it is necessary to know how long an interval of time τ after this earthquake one must consider in order to be reasonably sure of observing the next event in the sequence. I derive τ from a stochastic model of aftershock sequences. First, I assume Omori's law, which models the expected rate of aftershocks

$$a(t) = Ct^{-\alpha} \qquad t \geq t_0 \tag{7}$$

where t_0 is taken as 1 day, after which the catalog is presumed complete for magnitudes $M \geq M_{\min}$. I also assume that C is solely a function of the magnitude of the largest event of the sequence $M_{\max}$ and $M_{\min}$. Integrating (7) gives the expected number of events in the catalog from t_0 to T:

$$n(M_{\max}, M_{\min}, T) = \int_{t_0}^{T} C(M_{\max}, M_{\min}) t^{-\alpha}\, dt$$

Taking $\alpha = 1$ as a representative value [*Mogi*, 1962],

$$n(M_{\max}, M_{\min}, T) = C(M_{\max}, M_{\min}) \ln (T/t_0) \tag{8}$$

R. Stein (personal communication, 1982) empirically derived an expression relating C to the maximum and minimum magnitudes in the catalogs of aftershock sequences for seven mod-

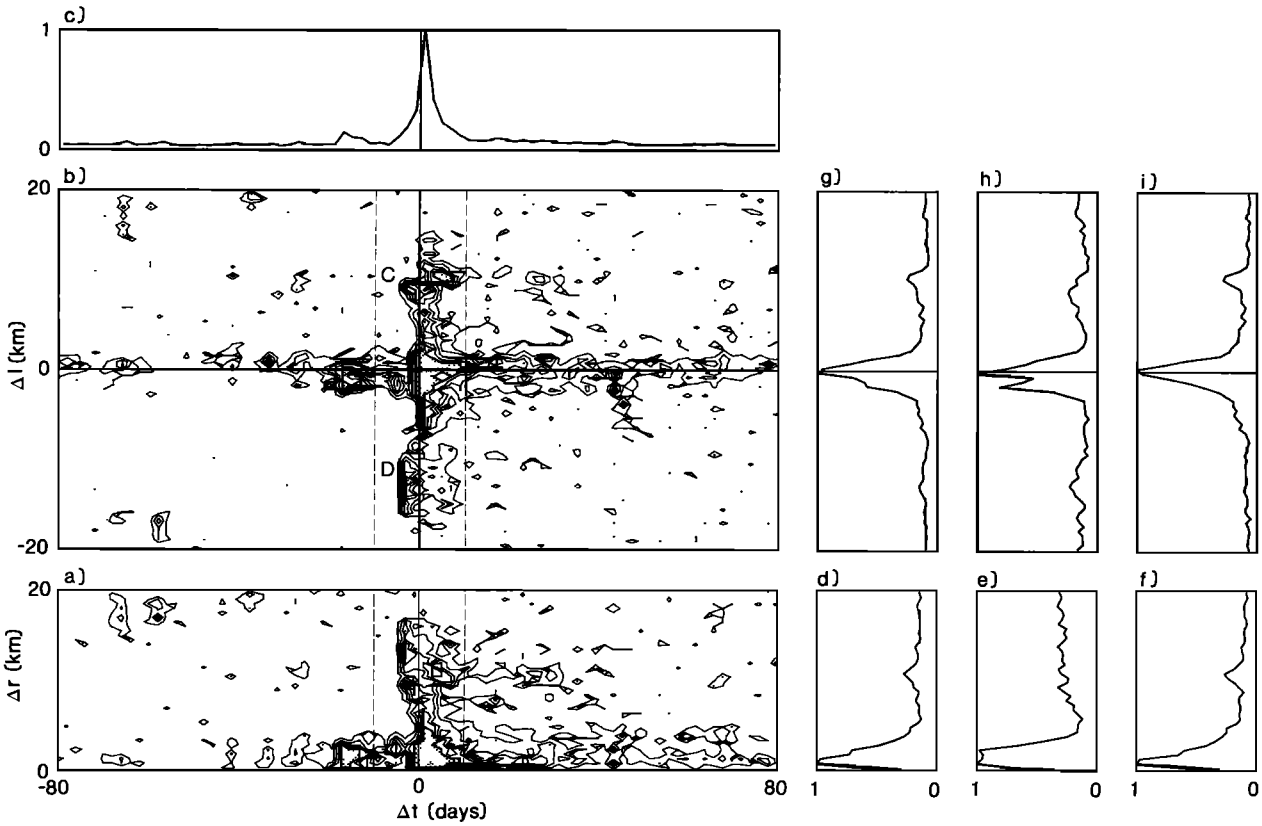

Fig. 6. Second-order moments and correlation functions for ranges indicated by dashed boxes in Figure 7. Dashed boxes indicate ranges shown in Figure 5. Cell size 0.5 km by 2 days in Figures 6*a* and 6*b*. Contour interval is 5 in Figure 6*a* and 4 in Figure 6*b*. See Figure 3 for further explanation.

erate to large earthquakes (six of them California events):

$$\log_{10} C = 2(M_{\max} - M_{\min} - 1)/3 \tag{9}$$

Adopting this relation and combining (7) and (9) gives the expected rate of aftershocks ($M_{\min} \le M \le M_{\max}$)

$$a(\Delta M, t) = 10^{2(\Delta M - 1)/3} t^{-1} \tag{10}$$

where $\Delta M = M_{\max} - M_{\min}$. I model an aftershock sequence as a time-dependent Poisson process with rate parameter $a = a(\Delta M, t)$. The probability of observing x earthquakes during the interval $(t, t + \tau)$ is given by

$$P(x, a(t), \tau) = \frac{e^{-a\tau}(a\tau)^x}{x!} \tag{11}$$

The probability of observing one or more events in the same interval is

$$P = \sum_{x=1}^{\infty} P(x, a(t), \tau) = 1 - P(0, a(t), \tau) = 1 - e^{-a(t)\tau}$$

$$= 1 - \exp\left[-10^{2(\Delta M - 1)/3}(\tau/t)\right] \tag{12}$$

Solving for τ,

$$\tau = \frac{-\ln(1 - P)t}{10^{2(\Delta M - 1)/3}} \tag{13}$$

determines the interval necessary to wait in order to be P confident of observing the next event in the sequence. For $P = 0.95$,

$$\tau = \frac{3t}{10^{2(\Delta M - 1)/3}} \tag{14}$$

Since τ is proportional to t, the time one must wait in order to be reasonably confident of observing the next event in the sequence is unbounded. An ideal upper bound for τ (for large t) would be one inversely scaled to the local background rate of seismicity. In the present formulation, however, a fixed bound of $\tau \le 10$ days was used. For earthquakes not already associated with a cluster, the value $\tau(t = 0) = 1$ day was adopted. These simplifications were made for the sake of computational efficiency and appear to have little effect on the results.

To assess the stability of the interaction model with respect to the modeling parameters, the cluster algorithm was repeatedly applied to a fixed subset of 3639 events with varying values of P and Q. Tables 1 and 2, respectively, show the number of clusters and number of events associated with a cluster resulting from these tests. Both the number of clusters and the number of events associated with a cluster are only weakly dependent on the value of Q over a range of four octaves, with increasing values of Q corresponding to increasing numbers of clusters and events clustered. The number of clusters and number of events clustered vary only slightly over a wide range of P (corresponding to the duration of interaction zones). However, for $P < 0.8$ (relatively brief interaction zones), the number of events associated with a cluster decreases while the number of clusters increases. This behavior reflects the fact that when the modeled interaction zone shortens, previously clustered sequences break up into smaller disconnected clusters and some events are dropped altogether from the clusters.

From these observations I conclude that the behavior of the cluster algorithm essentially reflects the space-time seismicity

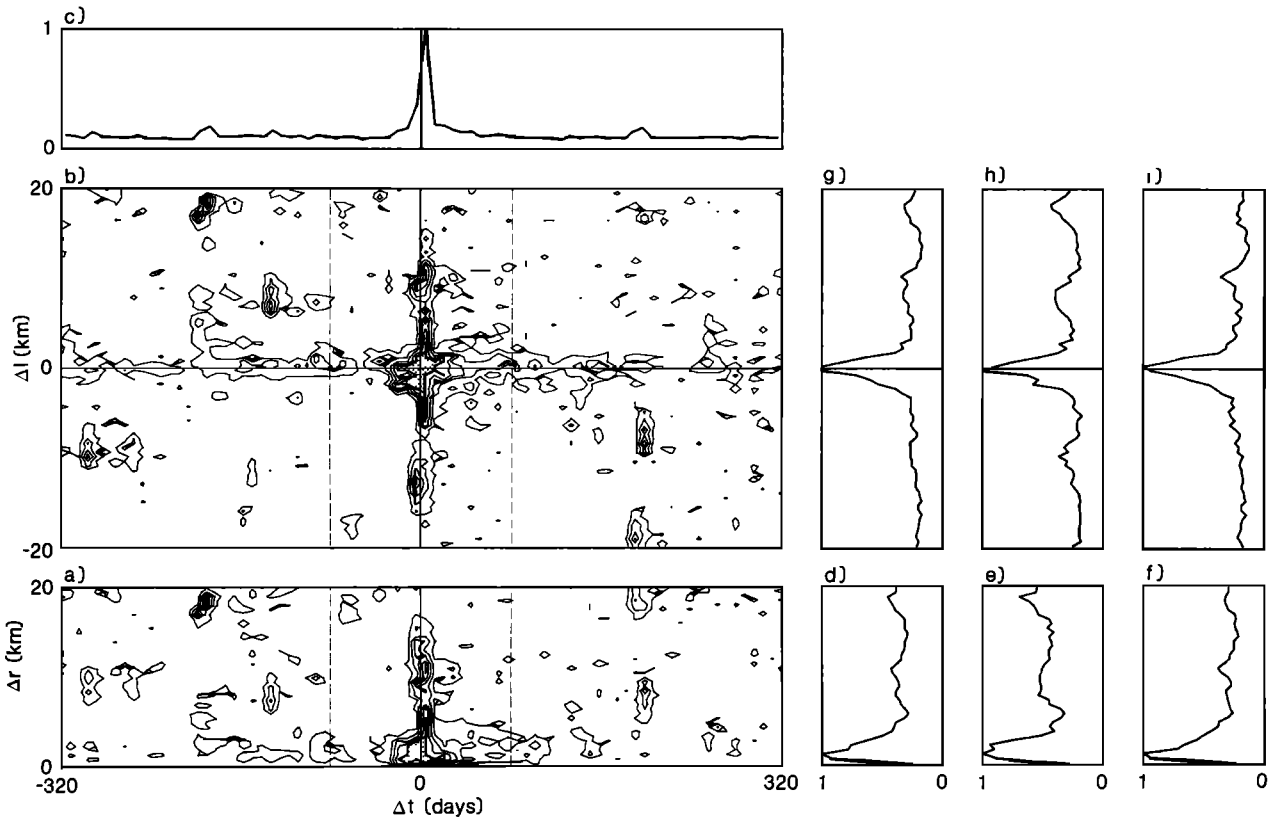

Fig. 7. Second-order moments and correlation functions for ranges indicated. Dashed boxes indicate ranges shown in Figure 6. Cell size 0.5 km by 8 days. Contour interval is 15 in Figure 7*a* and 10 in Figure 7*b*. See Figure 3 for further explanation.

patterns in the catalog and is relatively insensitive to the choice of interaction zone parameters. The resulting clusters are believed to represent the actual distribution of seismicity and are not considered to be artifacts of the modeling procedure. However, one should beware overinterpreting the detailed forms of individual identified clusters. Owing to the linking method employed by the algorithm, inclusion in or omission from the catalog of a few key events could in some cases result in a significant alteration in the shape of the cluster or in the fusing or fracturing of clusters.

Results for the Declustered Catalog

Application of the cluster algorithm to the 40,711 earthquakes within the study area resulted in the identification of 2686 clusters, including 48% of the catalog; the remaining events were not associated with any cluster. The distribution of cluster size is shown in Table 3. Although the distribution of clusters is dominated by the small clusters (90% contain five or fewer events), most of the clustered earthquakes are included in a few large clusters. The distribution of cluster duration (defined as the interval between the first and last event in a cluster) is peaked on a logarithmic scale between 0.1 and 1 day (Table 4); 82% of the clusters have durations less than 1 day. Thus the identified set of clusters is characterized by a two-event cluster of duration less than 1 day.

Visual inspection of the identified clusters (Figures 8 and 9) reveals that their space-time distribution with respect to the projection is highly variable, confirming a premise of this study that it is inappropriate to remove aftershocks from the catalog with a rectangular space-time window. Some unclustered events (pluses in Figures 8 and 9) appear to be embedded in clusters, but, in fact, are distant from the clusters and appear near due to epicentral and depth projection in these figures.

Figure 8 shows the clusters in box A in Figure 1 for a 2-year period including the complex sequence beginning with the 1972 Bear Valley (M_L 5.0) earthquakes and later involving the

TABLE 1. Relative Number of Clusters in Set of 3639 Events as a Function of Clustering Parameters, Relative to $P = 0.9$, $Q = 10$

	Q				
P	2	5	10	20	40
0.5	0.94	1.00	1.03	1.12	1.22
0.8	0.92	0.97	1.00	1.08	1.18
0.9	0.91	0.96	1.00	1.08	1.18
0.95	0.91	0.96	1.00	1.08	1.17
0.99	0.91	0.96	0.99	1.07	1.15

TABLE 2. Relative Number of Events Clustered in Set of 3639 Events as a Function of Clustering Parameters, Relative to $P = 0.9$, $Q = 10$

	Q				
P	2	5	10	20	40
0.5	0.87	0.94	0.97	1.04	1.14
0.8	0.93	0.96	1.00	1.07	1.18
0.9	0.93	0.97	1.00	1.07	1.18
0.95	0.93	0.97	1.00	1.08	1.18
0.99	0.94	0.97	1.01	1.08	1.18

TABLE 3. Distribution of Cluster Size

Number of Events in Cluster	Number of Clusters
2	1694
3	427
4	180
5	100
6	59
7	34
8	27
9	22
10	17
11	14
12	13
13	5
14	6
15	7
16	3
17	5
18	5
19	6
20	4
≥21	58

Largest cluster contains 4260 events. Total number of clustered events is 19,487. Total number of clusters is 2686.

1972 Stone Canyon (M_L 4.6) sequence some 10 km to the northwest. The fact that the cluster algorithm merged these sequences into one cluster shows that they are statistically related. However, the association of these sequences is apparently based on the mutual proximity of their respective aftershock zones and not on the basis of the initiation of the Stone Canyon sequence within the Bear Valley sequence's interaction zone. This observation fails to support the hypothesis by *Wesson* [1983] that the Stone Canyon sequence was triggered by afterslip from the Bear Valley sequence, if the afterslip zone is roughly identified by the aftershock zone. Of course, in view of the discussion on stability of the clustering algorithm in the previous section, this conclusion must be considered tentative since its basis lies in the interpretation of the specific shapes of the identified clusters.

Figure 9 shows the clusters located in box B in Figure 1 for a 2-year period including the Coyote Lake (790806; M 5.9) and Livermore (800124; M 5.9) earthquake sequences. (A stationary concentration at 90 km reflects quarry blasts near Los Altos.) The contrast in spatial development and duration between these clusters demonstrates the characteristic variability of earthquake sequences and the ability of the cluster algorithm to conform to the variations. The Coyote Lake aftershock cluster contains 180 events ($M \geq 1.5$) and ends 7.5 months after the main shock. Using the rectangular window method, *Reasenberg and Ellsworth* [1982] estimated the number of aftershocks ($M \geq 1.5$) to be 315. Within the aftershock zone they found that the seismicity rate decreased after the main shock according to $t^{-0.73}$ and estimated that it would return to background level some 20 months after the main shock [see *Reasenberg and Ellsworth*, 1982, Figure 10]. During the first 7.5 months of the sequence, 216 aftershocks are included in their window, 20% more than are included in the cluster for the same period. Since the zone used for these estimates is larger than the maximum extent of the aftershock zone and includes events at all depths within the zone, the resulting earthquake count may overestimate the aftershock population. The fact that the cluster algorithm cuts off at 7.5 months (some 12.5 months before the rate returns to background level) demonstrates a limitation of a stochastic model for aftershock identification. During the first 7.5 months the seismicity rate in the aftershock zone decreased from about 300 to 3 times background, followed by a decrease to the 10-year background rate between 7.5 and 20 months. During the latter period the Poisson probability that fluctuations in background seismicity exceed the observed rate increases from 0.002 to 0.5. Hence, while the seismicity rate in an aftershock zone asymptotically approaches the background rate, a "practical" cluster algorithm must cut off at a rate sufficiently above background to prevent a runaway instability.

The identified clusters thus represent the extent of a branching process based on a simple physical two-event model of earthquake interaction. How well this model corresponds to the actual physics of aftershock production is an essential question. The present model is undoubtedly oversimplified and fails to take into account important factors believed to control aftershock production, including geology and fault structure. Furthermore, seismogenic processes other than the aftershock process may also produce clusters satisfying the algorithm's criteria. Nevertheless, I assume here that the identified clusters represent only the aftershock process; then, from a statistical viewpoint all events in a cluster can be considered collectively as one independent event, along with the independent unclustered events. Accordingly, all the events in each cluster are replaced by an "equivalent event" whose origin time is that of the cluster's largest event, whose epicenter is the mean position of the cluster, and whose magnitude corresponds to the cumulative moment of the cluster. Figures 10 and 11 show space-time plots of the resulting "declustered" catalog corresponding to Figures 8 and 9, respectively. Most of the clustering apparent in Figures 8 and 9 has been removed, but some residual seismicity in the wake of the larger clusters is observed, probably reflecting incomplete aftershock identification as described in the previous paragraph. In the absence of clusters a weaker pattern of stationary spatial variation in event density along the fault zone is revealed. Relative maxima in spatial density occur at the latitudes of the Bear Valley (45–70 km, Figure 10) and Coyote Lake (20–40 km, Figure 11) sequences. However, this structure cannot be explained entirely by incomplete aftershock identification since, for the case of Bear Valley, it occurs both before and after the main shocks. Inspection of the declustered catalog over its 14-year span (not shown) reveals that variation in average earthquake productivity along the fault is a common and continuing feature of the catalog. For example, the relative minimum in seismic productivity at 50 km in Figure 11 persists throughout the 14-year catalog. Some of the space-stationary structures observed in the catalog may be controlled by quasi-constant factors including fault geometry and geology. Still others may be related to the particular pattern of stress re-

TABLE 4. Distribution of Cluster Duration

Duration of Cluster, days	Number of Clusters	Cumulative Number of Clusters
0.001– 0.009	524	524
0.01 – 0.099	617	1141
0.1 – 0.99	1063	2204
1. – 9.9	339	2543
10. – 99.	137	2680
100. –999.	5	2685
≥1000.	1	2686

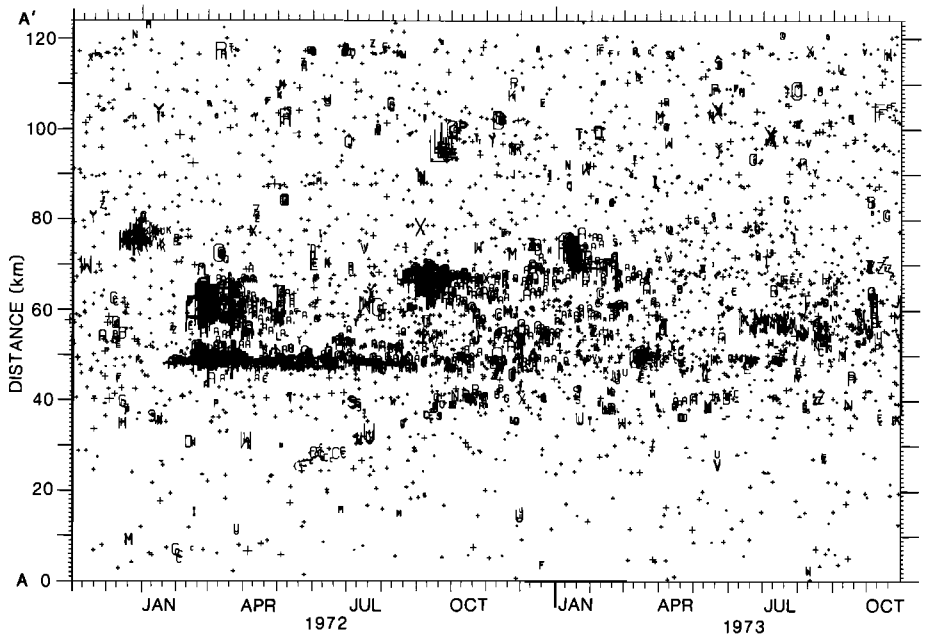

Fig. 8. Space-time diagram for seismicity located in box A, Figure 1. Epicenters are shown as a function of origin time and projected position on cross-section AA′ (Figure 1). Earthquakes plotted with like letter symbol belong to a single cluster. Letter symbols are reused. Unclustered events are plotted with plus signs. Symbol size indicates magnitude. The 1972 Bear Valley sequence occurs at 45–60 km starting in February 1972 and is followed in September by the Stone Canyon sequence 10 km to the northwest.

maining after the last great earthquake in 1906 on this portion of the San Andreas fault.

The second-order moments m_{2l} and m_{2r} were calculated for the declustered catalog over the same spatial and temporal ranges used for the raw catalog (compare Figures 12–16 with Figures 3–7, respectively). Replacement of the clusters by equivalent events reduced the number of pairs involved in these calculations an average of 77%. As a result, the contour levels in Figures 12–16 are lower. Over the ranges studied, the second-order moment for the declustered catalog is devoid of apparent structure. Repeat of the chi-square test on individual time sequences $n_{\Delta l}$ (Δt) showed that for all Δl the time sequences are consistent ($P = 0.90$) with a Poisson distribution. Inspection of the temporal correlation plots (Figures 12*b*, 13*b*, 14*b*, 15*b* and 16*b*) confirms the absence in the declustered catalog of second-order temporal correlation. Similarly, the

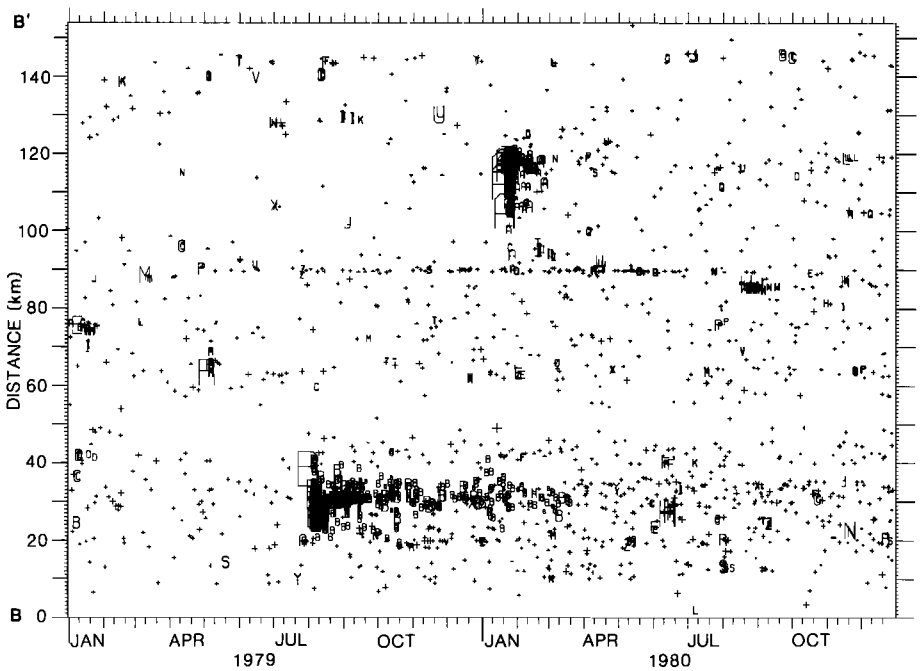

Fig. 9. Space-time diagram for seismicity located in box B, Figure 1. Epicenters are shown as a function of origin time and projected position on cross-section BB′ (Figure 1). See Figure 8 for further explanation. The Coyote Lake sequence (M 5.9, 790806, symbol B) and the Livermore sequence (M 5.9, 800124, symbol A) are prominent.

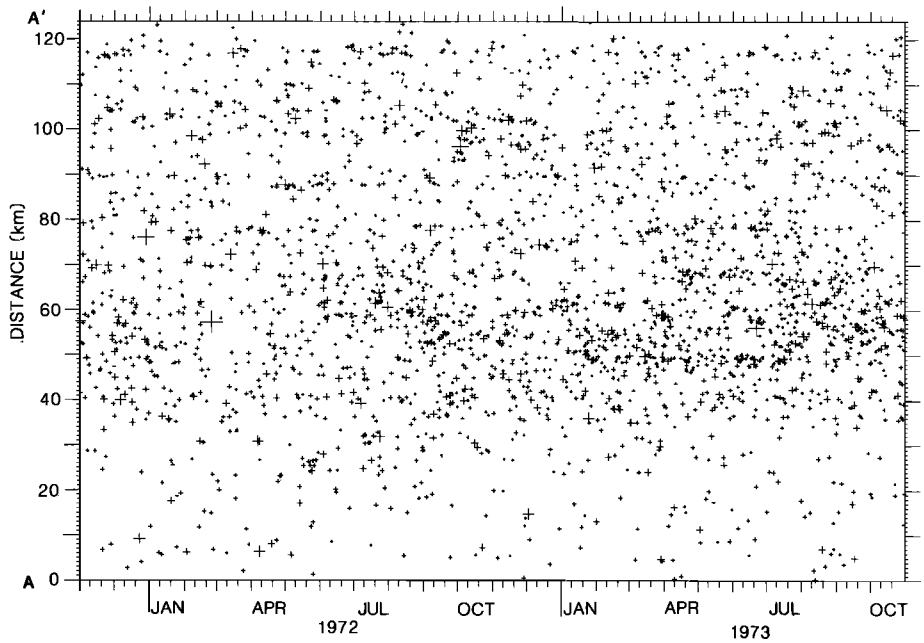

Fig. 10. Space-time diagram corresponding to Figure 8, but with events in each cluster replaced by an "equivalent event" (see text).

spatial correlation plots (Figures 12*c*–12*e* to 16*c*–16*e*) show that among foreshock-main shock pairs no second-order spatial structure remains in the declustered catalog. For main shock-aftershock pairs, however, a weak correlation for $\Delta l \leq 5$ km (Figures 12*e*, 13*e*, 14*e*, 15*e*, and 16*e*) may reflect an incomplete identification of aftershocks in that distance range. Slightly incomplete identification of aftershocks is an expected result owing to the early termination of aftershock sequences when their rate approaches the background rate, as discussed in the previous section.

DISCUSSION

I have modeled the occurrence of earthquakes in central California as a Poisson cluster process, in which random main events are accompanied by clusters of dependent events distributed about the main events according to their own probability distributions [*Kagan and Knopoff*, 1976; *Schlien and Toksoz*, 1970; *Vere-Jones*, 1970]. An assumption made, that the events identified by the cluster algorithm are totally dependent on their main shocks, led to the subsequent creation

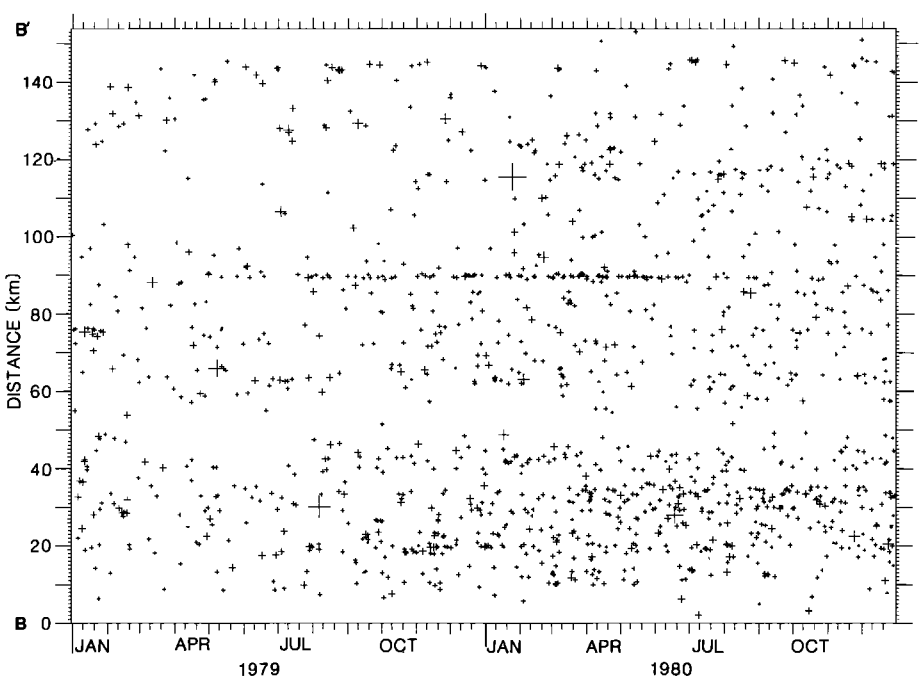

Fig. 11. Space-time diagram corresponding to Figure 9, but with all events in each cluster replaced by an "equivalent event" (see text).

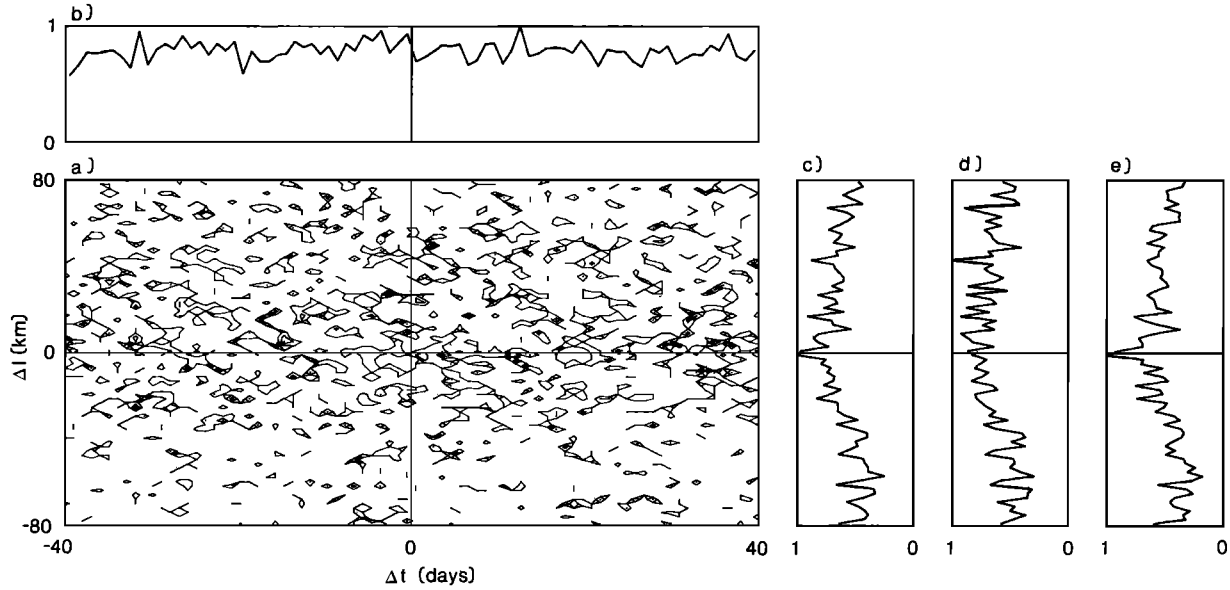

Fig. 12. Second-order moment and correlation functions for the "declustered catalog". (*a*) Second-order moment m_{2l}, corresponding to Figure 3*b*. Contour interval of 2 is smaller than in Figure 3*b* due to fewer number of pairs counted in moment for the declustered catalog. (*b*) Temporal correlation of earthquakes in the "declustered catalog", corresponding to Figure 3*c*. (*c*) Spatial correlation of earthquakes in the "declustered catalog" corresponding to Figure 3*g*. (*d*) Spatial correlation of earthquakes in the "declustered catalog" for foreshock-main shock parts, corresponding to Figure 3*h*. (*e*) Spatial correlation of earthquakes in the "declustered catalog" for main shock-aftershock pairs, corresponding to Figure 3*i*. See Figure 3 for further explanation.

of a random declustered catalog. A similar result was obtained for southern California seismicity by *Gardner and Knopoff* [1974]. No precursory information can be derived from the Poissonian component of the process (i.e., from the declustered catalog), and indeed no structure in the second-order moment of the declustered catalog was observed in this study. There remains, then, the question of the constituency of the identified clusters. Because no assumptions directly controlling cluster size, duration, shape, or location were made, these characteristics of the identified clusters bear investigation. For example, returning to the second-order moment of the raw catalog (Figure 3–7), an apparent relationship between the size of aftershock populations and the order of their occurrence is suggested by the present observations. Aftershock productivity appears to be enhanced for moderate earthquakes that are followed within 80 km and 40 days by another moderate earthquake. This supports the observation by *Keilis-Borok et al.* [1980] that earthquakes with abnormally large numbers of aftershocks tend to be precursors of a stronger earthquake. In both cases the productivity of aftershock sequences (C in equation (7)) increases prior to subsequent main shocks.

This last observation contradicts an implicit assumption in this work that the unclustered and equivalent events are statistically independent and that the identified aftershock popu-

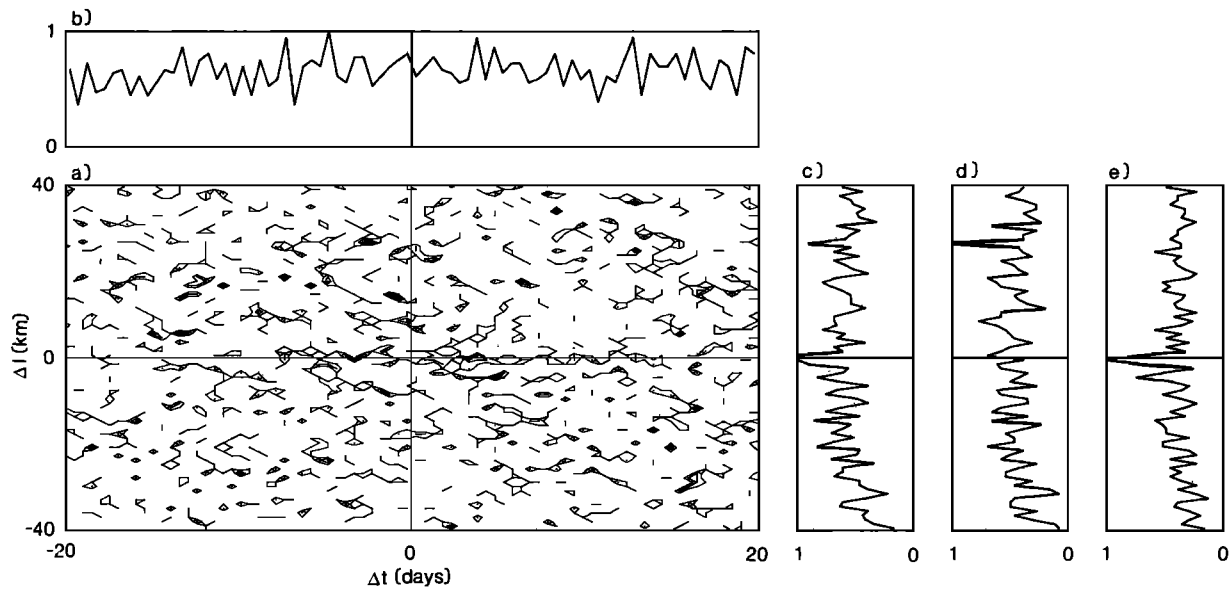

Fig. 13. Second-order moment m_{2l} and correlation functions for the "declustered catalog" over the ranges shown in Figure 4.

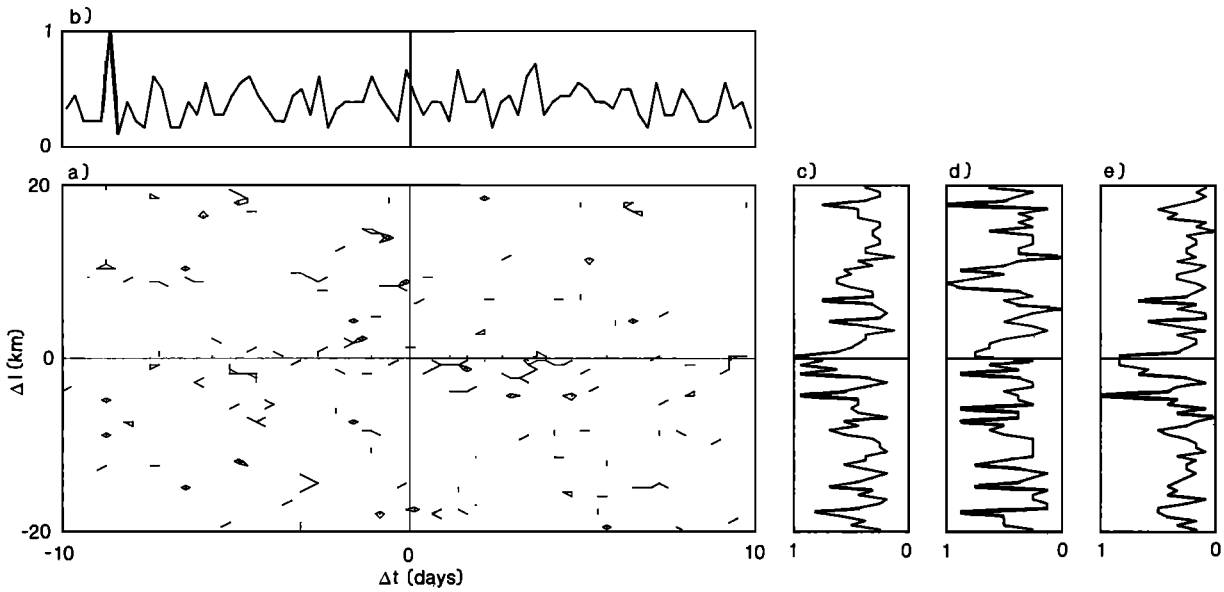

Fig. 14. Second-order moment m_{2l} and correlation functions for the "declustered catalog" over the ranges shown in Figure 5.

lations are solely dependent on their mainshock. To test directly the independence of the primary ($M \geq 4.0$) events, their autocorrelation function was calculated and is shown in Figures 17 and 18. Recall that the autocorrelation function is defined by (1) but calculated by drawing events for each pair (e_i, e_j) from the same set of $M \geq 4.0$ events. Figure 17 shows that over large interevent distances the primary events appear uncorrelated. Within a 20-km, 5-day window, however, a distinct pattern in the autocorrelation of primary events is present (Figure 18). Primary events tend to cluster with a characteristic southeast step (first event to second) along the fault system, with step length approximately 12 km and 3 days. This step relationship underlies the pattern (D) observed in Figure 4*b* on this scale. Figure 18 also shows a cluster at $\Delta l < 5$ km, $\Delta t < 1$ day which underlies the concentration in the cross correlation of the undeclustered catalog within these ranges discussed above.

Another question related to the use of the cluster algorithm (and interpretation of the declustered catalog) is What processes other than aftershocks are included in the clusters identified by the algorithm? The algorithm was designed to model the aftershock process. Both the assumption of Omori's Law in modeling the time dependence of the interaction zone and inclusion of the largest ancestor in modeling its spatial extent favor the identification of aftershock sequences over other types of clusters. It was demonstrated that the aftershock clusters are removed by the algorithm nearly completely (given the stochastic nature of seismicity) and efficiently: fewer than half the events in the catalog are included in the clusters. This compares with the approximately two thirds of the southern California catalog that was identified as aftershocks by *Gardner and Knopoff* [1974] using the window method. However, there is evidence that foreshocks are also included in the clusters. In 38% of the identified clusters the second-largest event

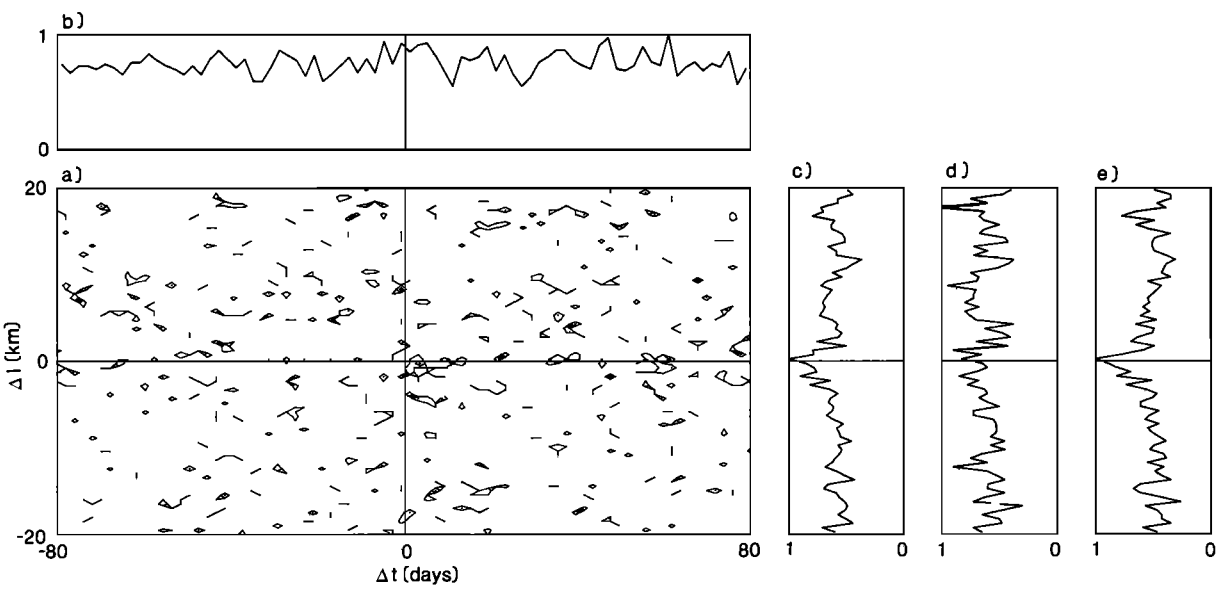

Fig. 15. Second-order moment m_{2l} and correlation functions for the "declustered catalog" over the ranges shown in Figure 6.

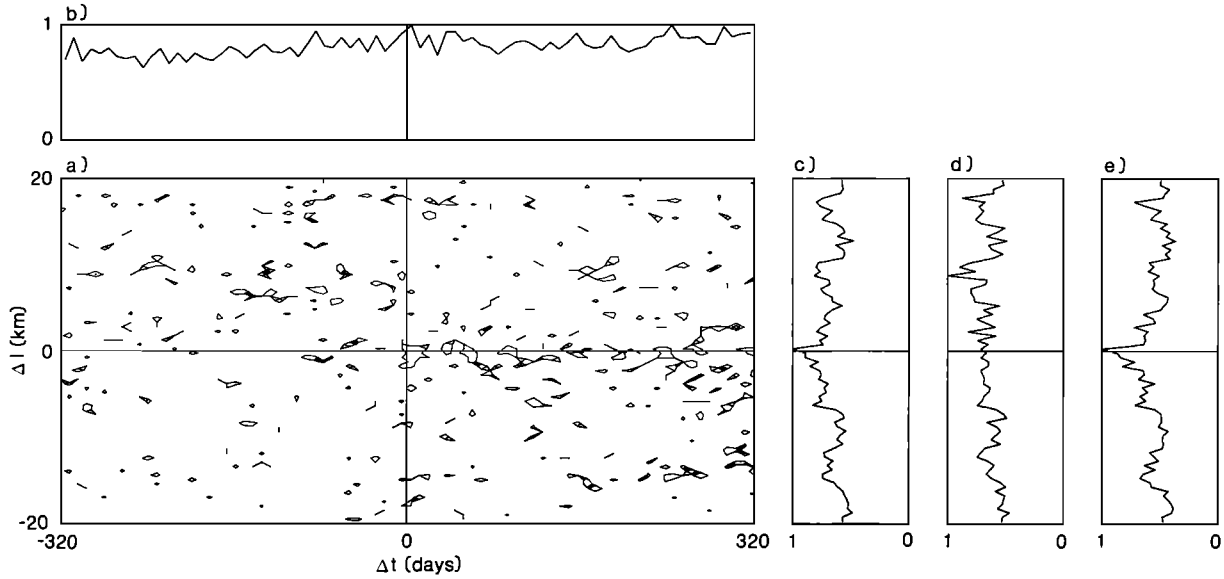

Fig. 16. Second-order moment m_{2l} and correlation functions for the "declustered catalog" over the ranges shown in Figure 7.

precedes the largest event, indicating foreshocklike behavior. An example of foreshock inclusion in a cluster is apparent in Figure 8, where a precursory swarm beginning in late January 1972 is included in the main Bear Valley sequence cluster. Pertaining to the task of identifying and removing aftershocks, it appears to be a shortcoming of the cluster method that foreshocklike sequences are identified together with the aftershocklike ones. However, the result demonstrates that the distinction between the two is really a gradual one, with many clusters containing both foreshocks and aftershocks. Perhaps the common method of identifying and removing aftershocks so that the residual catalog may be analyzed might better be reformulated to one of identifying and analyzing the clusters while ignoring the random background component of the seismicity on which they are superimposed.

We return now to the question of significance of the pattern of foreshock activity observed in m_{2l} and m_{2r} at Δr, $\Delta l \lesssim 15$ km, $\Delta t \leq 3$ days (C and D in Figures 4–6). Recall that no claim was made for the statistical significance of these features. Nevertheless, for several reasons features C and D are interesting. Their spatial extent (12–15 km) is approximately twice that of the aftershocks for the same set of main shocks (compare Figures 5*a* and 5*f*). Their temporal extent ($\sim$3 days) agrees well with the mean precursor time $10^{0.65\pm1.1}$ days (limits represent 1 standard deviation) determined by *Rikitake* [1979] for precursors of the third kind to $M \geq 6$ earthquakes.

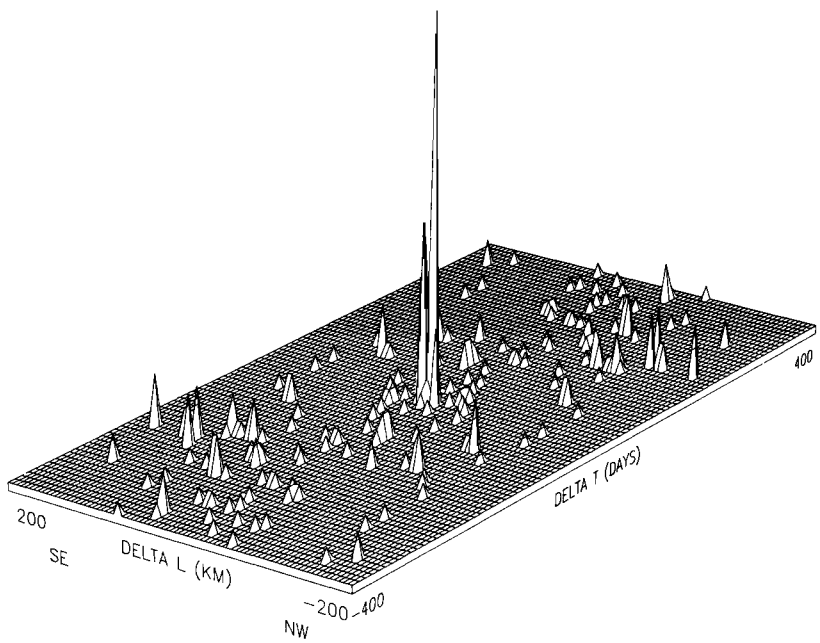

Fig. 17. Autocorrelation of $M \geq 4.0$ earthquakes over interevent distances up to 200 km and interevent times up to 400 days. Height of surface is proportional to the number of pairs in the catalog for given interevent separation. Largest peak (at origin) corresponds to the 46 self-pairs (e_i, e_i). Autocorrelation function is point symmetric with respect to origin, by definition.

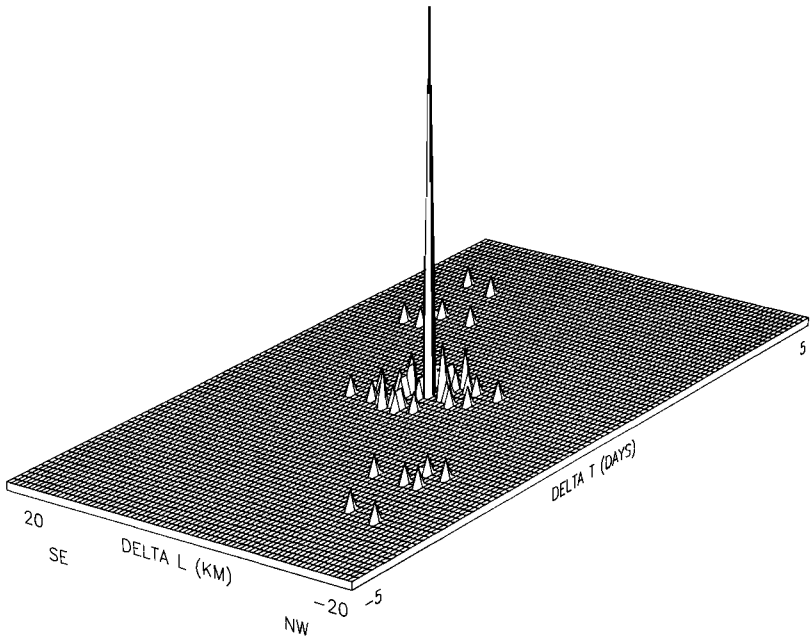

Fig. 18. Autocorrelation of $M \geq 4.0$ earthquakes over interevent distances up to 20 km and interevent times up to 5 days. See Figure 17 for further explanation.

And the suggested range of migration velocity of 2.6–5.3 km/d is comparable with the rates 7.7 and 3.8 km/d for foreshocks and aftershocks, respectively, of large ($M \geq 7$) earthquakes observed by *Kagan and Knopoff* [1976]. If this is the case, failure of the chi-square test to detect their significance (after removal of the clusters) could be explained by an error in the assumption that the identified clusters are only dependent upon their respective main shocks. If the clusters are not independent of the unclustered seismicity, as *Keilis-Borok et al.* [1980] suggested, then the statistical model we have used (Poisson clustered process with clusters defined by the present algorithm) to determine significance is inappropriate and is not a valid basis for assessing statistical significance of these features. An implication of this conclusion is that precursory information may be present in the behavior (specifically, productivity) of aftershock sequences. Generally, aftershock sequences are considered to be (and modeled as) dependent processes related solely to their respective main shocks. Their removal invariably results in a random residual catalog. If, however, the aftershock process is telling us something about the readiness of the crust for another main shock, then analysis, rather than removal, of accurately identified aftershock sequences may be a productive approach toward earthquake prediction.

Summary and Conclusions

1. A dominant feature of the second-order moment of central California seismicity (1969–1982) is the presence of clustering apparently related to the aftershock process. This process obscures the statistical expression of weaker processes, including precursory ones.

2. While based on only a few examples and not statistically significant under present assumptions about the dependency of aftershocks, an observed intensification of foreshock activity within 15 km and 3 days of $M \geq 4.0$ main shocks suggests a precursory process with weak microseismic expression at this length and time scale. Migration toward epicenter at 2.6–5.3 km/d is suggested by the data.

3. An algorithm for recognizing aftershock clusters based on a simple two-event model of earthquake interaction identified 48% of the events in the catalog as aftershocks. The model makes no assumption regarding the extent, duration, or "shape" of clusters. It appears to have successfully adapted to the wide variations in cluster geometry present in the catalog.

4. When all the events in each identified cluster are replaced by an "equivalent event" (i.e., when the catalog is declustered), the resulting catalog displays weak time-stationary variations in average seismic productivity along the strike of the San Andreas fault zone. These variations probably result from variations in geology and fault geometry.

5. The second-order moment of the declustered catalog is Poissonian in space and time over ranges of interevent distance up to 80 km and interevent time up to 320 days.

6. Autocorrelation of $M \geq 4.0$ earthquakes in central California indicates a southeast propagating steplike migration with characteristic step length approximately 12 km and 3 days.

7. Aftershock productivity of moderate earthquakes may be enhanced for main shocks that are followed by another moderate main shock within 80 km and 40 days. This result, based on a small number of examples, suggests that aftershock productivity may be a predictor of future nearby earthquakes. A similar conclusion was reached by *Keilis-Borok et al.* [1980] for $M \geq 6.5$ earthquakes in southern California.

Acknowledgments. I gratefully acknowledge many helpful and stimulating discussions with J. Andrews, W. Ellsworth, T. Habermann, L. Jones, Y. Kagan, A. Lindh, D. Oppenheimer, and R. Stein. The clustering algorithm evolved from an earlier program written by W. Savage and W. Ellsworth. I thank J. Dewey, T. Habermann, L. Jones, Y. Kagan, and C. Weaver for constructively critical and thorough reviews of the manuscript.

References

Bakun, W. H., Seismic moments, local magnitudes, and coda-duration magnitudes for earthquakes in central California, *Bull. Seismol. Soc. Am.*, *74*, 439–485, 1984.

Cox, D. R., and P. A. W. Lewis, *The Statistical Analysis of Series of Events*, 285 pp., Methuen, London, 1966.

Daley, D. J., and D. Vere-Jones, A summary of the theory of point processes, in *Stochastic Point Processes: Statistical Analysis, Theory and Applications*, edited by P. A. W. Lewis, pp. 299–383, John Wiley, New York, 1972.

Ellsworth, W. L., Bear Valley, California, earthquake sequence of February–March 1972, *Bull. Seismol. Soc. Am.*, *65*, 483–506, 1975.

Gardner, J. K., and L. Knopoff, Is the sequence of earthquakes in southern California, with aftershocks removed, Poissonian? *Bull. Seismol. Soc. Am.*, *64*, 1363–1367, 1974.

Kagan, Y. Y., Spatial distribution of earthquakes: The three-point moment function, *Geophys. J. R. Astron. Soc.*, *67*, 697–717, 1981*a*.

Kagan, Y. Y., Spatial distribution of earthquakes: The four-point moment function, *Geophys. J. R. Astron. Soc.*, *67*, 719–733, 1981*b*.

Kagan, Y., and L. Knopoff, Statistical search for non-random features of the seismicity of strong earthquakes, *Phys. Earth Planet. Inter.*, *12*, 291–318, 1976.

Kagan, Y. Y., and L. Knopoff, Spatial distribution of earthquakes: The two-point correlation function, *Geophys. J. R. Astron. Soc.*, *62*, 303–320, 1980.

Kanamori, H., The nature of seismicity patterns before large earthquakes, in *Earthquake Prediction, An International Review, Maurice Ewing Ser.*, vol. 4, edited by D. W. Simpson and P. G. Richards, pp. 1–19, AGU, Washington, D. C., 1981.

Kanamori, H., and D. L. Anderson, Theoretical basis of some empirical relations in seismology, *Bull. Seismol. Soc. Am.*, *65*, 1073–1095, 1975.

Keilis-Borok, V. I., L. Knopoff, I. M. Rotvain, and T. M. Siderenko, Bursts of seismicity as long-term precursors of strong earthquakes, *J. Geophys. Res.*, *85*, 803–811, 1980.

Knopoff, L., and J. K. Gardner, Higher seismic activity during local night on the worldwide earthquake catalog, *Geophys. J. R. Astron. Soc.*, *28*, 311–313, 1972.

McNally, K., Spatial, temporal and mechanistic character in earthquake occurrence, Ph.D. thesis, Univ. of Calif., Berkeley, 1976.

Mogi, K., On the time distribution of aftershocks accompanying the recent major earthquakes in and near Japan, *Bull. Earthquake Res. Inst. Univ. Tokyo*, *40*, 107–124, 1962.

Prozorov, A. G., and A. M. Dziewonski, A method of studying variations in the clustering property of earthquakes: Application to the analysis of global seismicity, *J. Geophys. Res.*, *87*, 2829–2839, 1982.

Reasenberg, P., and W. L. Ellsworth, Aftershocks of the Coyote Lake, California, earthquake of August 6, 1979: A detailed study, *J. Geophys. Res.*, *87*, 10,637–10,655, 1982.

Rikitake, T., Classification of earthquake precursors, *Tectonophysics*, *54*, 293–309, 1979.

Savage, W. U., Microearthquake clustering near Fairview Peak, Nevada, and in the Nevada seismic zone, *J. Geophys. Res.*, *77*, 7049–7056, 1972.

Schlien, S., and M. N. Toksoz, A clustering model for earthquake occurrences, *Bull. Seismol. Soc. Am.*, *60*, 1765–1787, 1970.

Vere-Jones, D., Stochastic models for earthquake occurrence, *J. R. Stat. Soc., Ser. B*, *32*, 1–62, 1970.

Vere-Jones, D., Space-time correlations for microearthquakes—A pilot study, *Adv. Appl. Probab.*, suppl., *10*, 73–87, 1978.

Wesson, R. L., Aftershocks and afterslip (abstract), *Eos Trans. AGU*, *64*, 766, 1983.

Wesson, R. L., and W. L. Ellsworth, Seismicity preceding moderate earthquakes in California, *J. Geophys. Res.*, *78*, 8527–8546, 1973.

P. Reasenberg, U.S. Geological Survey, 345 Middlefield Road, MS/77, Menlo Park, CA 94025.

(Received September 13, 1984;
revised January 22, 1985;
accepted February 11, 1985.)